Astron. Astrophys. 362, 158–168 (2000)

ASTRONOMY AND ASTROPHYSICS

CO band emission from MWC 349

I. First overtone bands from a disk or from a wind?

M. Kraus[1], **E. Krügel**[1], **C. Thum**[2], **and T.R. Geballe**[3]

[1] Max-Planck-Institut für Radioastronomie, Auf dem Hügel 69, 53121 Bonn, Germany
[2] Institut de Radio Astronomie Millimetrique, 38406 Saint Martin d'Hères, France
[3] Gemini Observatory, 670 North A'ohoku Place, University Park, Hilo, HI 96720, USA

Received 16 December 1999 / Accepted 26 July 2000

Abstract. We have obtained spectra in the K band of the peculiar B[e]-star MWC 349. A 1.85–2.50 μm spectrum, measured at medium resolution, contains besides the strong IR continuum the first overtone CO bands, the hydrogen recombination lines of the Pfund series, and a number of other neutral atomic lines and ionic lines of low ionization, all in emission. Portions of the CO band and superposed Pfund series lines were observed at resolutions of 10–15 km s^{-1}. The Pfund lines have gaussian profiles with FWHMs of ~ 100 km s^{-1}, are optically thin, and are emitted in LTE. The CO band heads are formed in LTE at temperatures of 3500 to 4000 K. The width of the $2 \rightarrow 0$ band head indicates kinematic broadening of 50 to 60 km s^{-1}. A number of CO emission geometries were investigated by spectral modeling. The emission may occur at the inner edge of the rotating circumstellar disk. In this case, the disk must have an outer bulge which partly blocks the radiation so that the observer sees only a sector on the far side where radial velocities are small. Alternatively, the CO emission originates in a wind and lines have gaussian profiles. Fits to both these geometries are of equally good quality. In a third alternative where the fit is less convincing, the CO emission is optically thin and comes from an extended Keplerian disk. In all successful fits the CO column density is $\sim 5 \cdot 10^{20}$ cm^{-2}.

Key words: line: formation – stars: circumstellar matter – stars: emission-line, Be – infrared: stars – stars: individual: MWC 349

1. Introduction

After the discovery of CO band head emission in the BN object by Scoville et al. (1979) a large number of further detections in other young stellar objects (YSOs) followed (see e.g. Geballe & Persson 1987; Carr 1989; Chandler et al. 1993; Greene & Lada 1996; Najita et al. 1996).

Several scenarios were discussed to explain the origin of the hot (2500–5000 K) and dense ($n > 10^{11}$ cm^{-3}) CO component in YSOs (for some examples see Calvet et al. 1991; Martin 1997), but the most likely location is a neutral disk or wind (Carr 1989; Chandler et al. 1995). The disk model is especially supported by high resolution spectroscopic observations of the CO $2 \rightarrow 0$ band head. For several young stellar objects the shape of this band head shows the kinematic signature of Keplerian rotation (Carr et al. 1993; Carr 1995; Najita et al. 1996) and is a powerful tracer for the existence of a circumstellar disk around YSOs.

The peculiar B[e]-star MWC 349 also shows the first overtone CO bands in emission, first observed by Geballe & Persson (1987) at a velocity resolution of about 460 km s^{-1}. MWC 349 is a binary system consisting of the main component MWC 349A, classified as a B[e]-star, and the B0 III companion, MWC 349B, located 2″ west of MWC 349A. Here we are only interested in the main component, in the following referred to as MWC 349. Its evolutionary state is still unclear. It shows some characteristics of a pre-main sequence B[e]-type star as well as characteristics of a B[e] supergiant (e.g. Lamers et al. 1998). Cohen et al. (1985) determined its distance (1.2 kpc), bolometric luminosity ($\sim 3 \cdot 10^4$ L$_\odot$) and the visual extinction towards it ($A_{\rm V}^{\rm ISM} \simeq 10$ mag of which 2 mag might be circumstellar).

The existence of a bulge of circumstellar dust around MWC 349 has been known for decades (e.g. Geisel 1970). The proposition that MWC 349 also has a disk is supported by observations of double-peaked emission lines (Hamann & Simon 1986, 1988) and by IR speckle interferometry (Leinert 1986; Mariotti et al. 1983) which revealed a disk-like structure of emission by dust, elongated in the east-west direction and seen nearly edge on. An accumulation of neutral gas and dust in the equatorial plane of the star is believed to be responsible for the bipolar structure of the optically thick wind zone seen in the VLA-map of White & Becker (1985). The mass loss rate found for a 50 km s^{-1} wind velocity is $\sim 1.2 \cdot 10^{-5}$ M$_\odot$ yr^{-1} (Cohen et al. 1985).

Another indicator for the circumstellar disk is the strong hydrogen recombination maser line emission in the mm and submm range, which also shows the characteristic double-peaked profiles (e.g. Martín-Pintado et al. 1989). Recombination lines at different wavelengths sample different regions. With decreasing quantum number n, i.e. increasing frequency, one sees ionized gas closer to the star. The fact that the rotational

Send offprint requests to: M. Kraus (mkraus@mpifr-bonn.mpg.de)

Table 1. Identified lines in the NIR spectrum of MWC 349 (Figs. 1a and b).

number	wavelength [μm]	line identification
1	1.86904	He I
2	1.87561	Paα
3	1.89282	C I, Ca I
4	1.90867	He I
5	1.94508	Brδ, Ca I
6	1.95445	N I
7	1.97470	Si I, C I, N I
8	1.98702	Ca I, C I
9	1.99318	Ca I, Si I, C I
10	2.00130	C I
11	2.05917	He I
12	2.08819	(?) Sn I, Fe II
13	2.11194	He I
14	2.13831	Mg II, C I, Si I
15	2.14359	Mg II, Ca II, [Fe III]
16	2.16611	Brγ
17	2.20687	Na I doublet, Si I, (?) O II
18	2.21741	C I
19	2.24113	(?) Fe II

velocity of recombination lines displays a systematical increase with decreasing n suggests that the maser emission originates in the ionized atmosphere of a Keplerian disk around a 25–30 $M_\odot$ star (Thum et al. 1992; Thum et al. 1994). In addition, Rodríguez & Bastian (1994) determined the inclination angle of the disk towards the line of sight to be $15° \pm 5°$.

In this paper, we present a new medium resolution spectrum of the K band, which includes hydrogen recombination line emssion and first overtone CO band emission. We also present high resolution observations encompassing the regions of the $2 \rightarrow 0$ and $3 \rightarrow 1$ CO band heads. We discuss the probable location of the hot CO by modeling its emission for several geometries.

2. Observations

On 1997 August 2 (UT) we observed MWC 349 at the United Kingdom 3.8 m Infrared telescope (UKIRT) telescope at 1.85–2.5 μm, using the facility spectrometer CGS4 with a spectral resolution of $\sim 330\,\mathrm{km\,s^{-1}}$ (Fig. 1a). The F4V star HR 7550 was used as a flux calibrator; we assumed for it a surface temperature of 6600 K and a K magnitude of 5.5. Wavelength calibration was provided by a spectrum of an argon lamp. The spectrum contains several prominent hydrogen and helium recombination lines as well as the first overtone CO bands, all of them in emission. Those shortward of 2.25 μm are given in Table 1.

On 1998 June 24 and August 5 we use the echelle in CGS4 to reobserve MWC 349 in the spectral range 2.285–2.341 μm at much higher spectral resolution (10–15 $\mathrm{km\,s^{-1}}$). HR 7924 (α Cygni) served as the calibration star and telluric absorption lines and arc lamp lines served as wavelength calibrators. The observations consisted of four separate, contiguous, oversampled subspectra with small overlaps. To improve the signal-to-noise ratio we binned each spectrum to roughly one data point per resolution element. To make the subspectra consistent with (Fig. 1c) required that each one be scaled by a factor near unity.

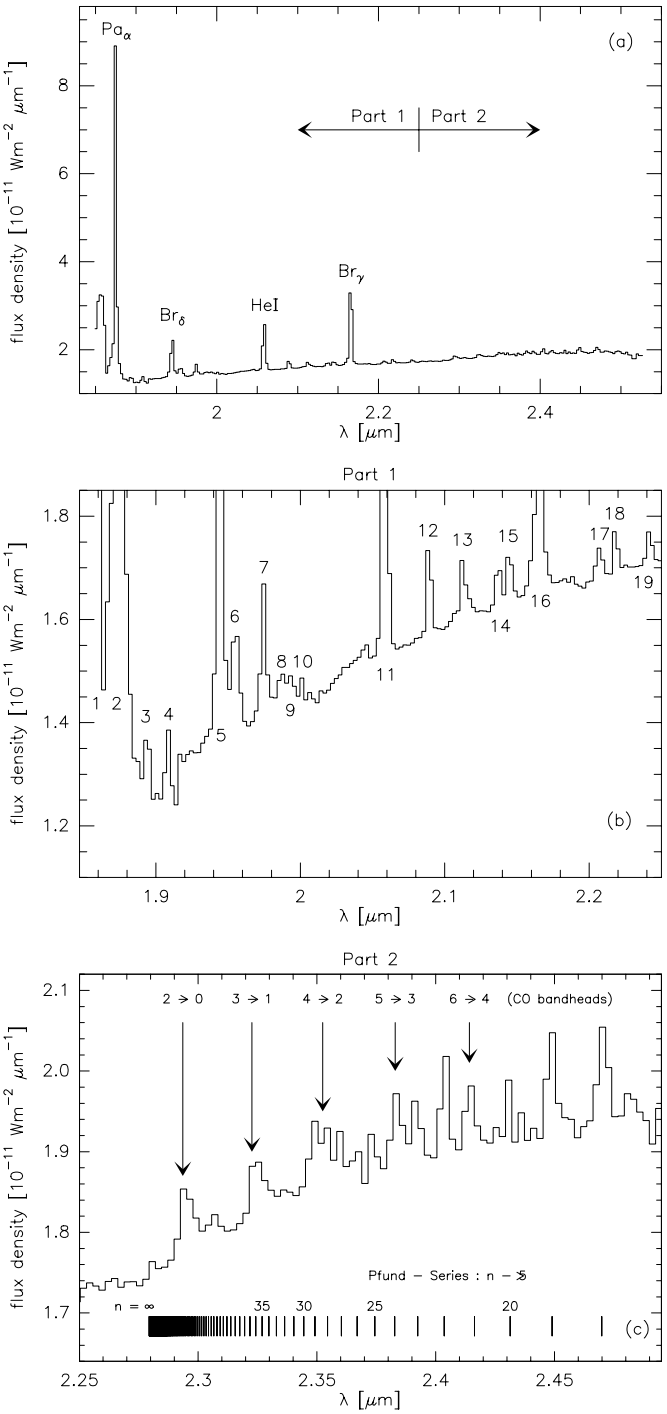

Fig. 1a–c. For better visualization, the 1.85–2.50 μm spectrum of MWC 349 observed at UKIRT with a spectral resolution of $\sim 330\,\mathrm{km\,s^{-1}}$ (upper panel) is split in two parts: Part 2 (bottom panel) contains the first overtone CO bands (indicated by the arrows) and most lines from the Pfund series of the hydrogen atom (vertical bars), the remaining spectrum (Part 1, middle panel) contains several emission lines listed in Table 1.

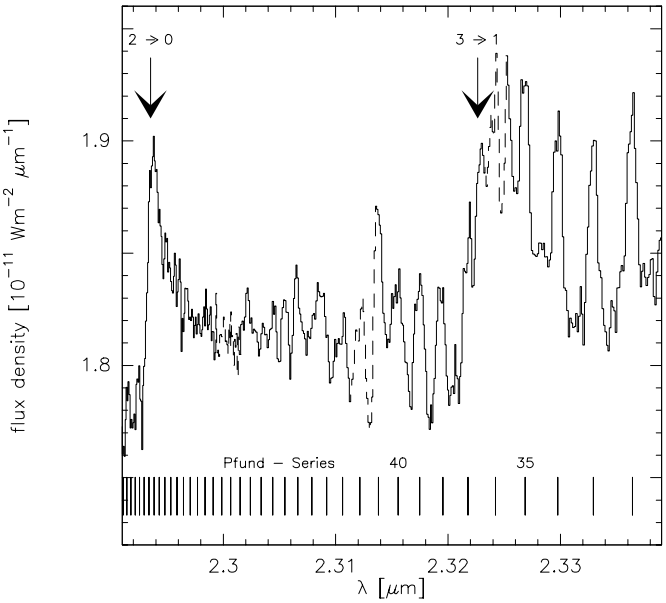

Fig. 2. High resolution spectrum of MWC 349 near the first two CO band heads. The dashed regions mark the overlap for pairs of adjacent subspectra where the flux calibration is rather uncertain.

We then combined them to produce the spectrum in Fig. 2. The $3 \rightarrow 1$ band head falls into the overlap region of two subspectra, so its strength is rather uncertain (marked by the dashed line within the figure). This causes increased uncertainty in the modeling of the spectrum.

3. Hydrogen recombination lines – the Pfund series

As can be seen in Figs. 1c and 2, the 2.25–2.5 μm spectrum of MWC 349 contains both the first overtone CO bands and the Pfund series (transitions of the form $n \rightarrow n' = 5$, denoted as Pf(n)) of the hydrogen atom. Hamann & Simon (1986) already identified some of them in their velocity-resolved infrared spectroscopy of MWC 349, but their resolution of $\sim$20 km s^{-1} was lower than that of our echelle spectrum, so they could only resolve lines up to Pf(34). The FWHMs they derived from several unblended lines are about 100 km s^{-1} and agree with our values.

Many of the emission lines observed by Hamann & Simon (1986) are double-peaked, which hints at a rotating medium. The Pfund lines which we have observed at high resolution are superimposed on the CO bands. Their profiles look more like gaussians. A gaussian velocity component of about 50 km s^{-1} FWHM would not be surprising, as the centimeter and mid-IR hydrogen recombination lines as well as the 'pedestal' feature of the double-peaked mm recombination maser lines contain such a velocity component (Smith et al. 1997; Thum et al. 1992). The gaussian component often is ascribed to the wind of MWC 349.

To model the hydrogen emission, we assume the Pfund lines to be optically thin. Their intensities are given by

$$I_\nu = N_n A_{n,5} h\nu \, \Phi_{\rm H}(\nu) \; . \tag{1}$$

To evaluate this, the number density N_n of the atoms in level n, the Einstein coefficients, $A_{n,5}$, and the line profile for hydrogen, $\Phi_{\rm H}(\nu)$, are required.

In view of the measured line widths, we choose the gaussian profile,

$$\Phi_{\rm H}(\nu) = \frac{1}{\sqrt{\pi}\frac{\nu_0}{c}v} \, \exp\left[-\left(\frac{\nu-\nu_0}{\frac{\nu_0}{c}v}\right)^2\right] \tag{2}$$

in which v is the most probable velocity, given by $v = \sqrt{2kT/m}$ for a Maxwellian velocity distribution. In our case, $v \simeq 50$ km s^{-1}. We also take into account the local standard of rest velocity of ~ 8 km s^{-1} (Thum et al. 1992; Thum et al. 1995).

The Einstein coefficients, $A_{nn'}$, can be calculated, following Menzel & Pekeris (1935). For Pfund lines with $n \geq 18$ (see Fig. 1c), they can be approximated by

$$A_{n,5} \simeq 3.023 \cdot 10^9 \; n^{-5.005} \; . \tag{3}$$

The number density, N_n, of the level n follows from Saha's equation

$$N_n = b_n N_{\rm i} N_{\rm e} g_n \, \frac{h^3}{2\,(2\pi m_{\rm e} k T_{\rm e})^{3/2}} \, {\rm e}^{\frac{h\,Ry}{n^2 k T_{\rm e}}} \tag{4}$$

where $N_{\rm i}$ and $N_{\rm e}$ are the number densities of the protons and electrons, $T_{\rm e}$ and $m_{\rm e}$ are the electron temperature and electron mass, $g_n = 2n^2$ is the statistical weight of state n, and Ry is the Rydberg constant. The b_n-factors which describe the deviation from LTE and which depend on the electron temperature and density were taken from the electronic tables of Storey & Hummer (1995) for Menzel case B recombination.

Detailed modeling of the Pfund line spectrum performed by Kraus (2000) shows that the emission arises within the innermost parts of the ionized wind where the electron densities are highest. Within these regions it is expected that $N_{\rm e} \leq 10^9$ cm^{-3}. Electron densities as high as 10^8 cm^{-3} have already been found by Strelnitski et al. (1996) and Thum et al. (1998). For such high densities the emission is clearly in LTE, i.e. the b_n-factors are ~ 1, and non-LTE effects are negligible.

In our case of optically thin Pfund lines in LTE and at a constant electron temperature, the intensity ratio of neighbouring Pfund lines independent of the electron density is according to Eq. (1),

$$\frac{I_{{\rm Pf}(n+1)}}{I_{{\rm Pf}(n)}} \sim \left(\frac{n}{n+1}\right)^{5.005} \cdot \exp\left(-\frac{hRy}{kT_{\rm e}}\frac{2n+1}{(n^2+n)^2}\right) \; . \tag{5}$$

and always smaller than 1, implying that the intensity of the Pfund lines decrease with increasing quantum number. This behaviour can be seen in Fig. 3 where synthetic spectra of Pfund lines smoothed to spectral resolutions of 10–15 km s^{-1} and 330 km s^{-1} are plotted near the series limit. The wavelength difference between the neighbouring Pfund lines decreases with increasing n leading to a blend of the individual lines at short wavelengths. The onset of this blend, which depends on the width of the lines and on the spectral resolution, leads to a hydrogen 'continuum'.

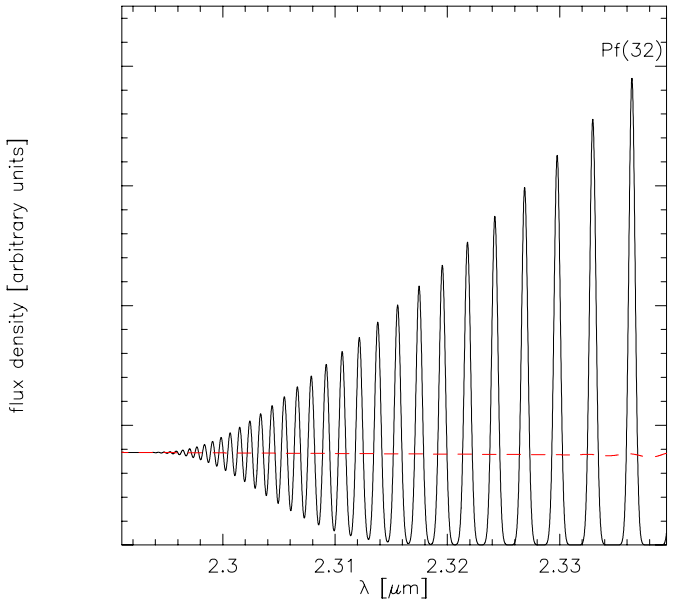

Fig. 3. Spectrum of optically thin Pfund lines in LTE, with an isothermal electron temperature of $T_\mathrm{e} = 10^4$ K and a gaussian velocity component of 50 km s^{-1}. The spectral resolutions to which the raw spectrum was convolved are 330 km s^{-1} (dashed line) and 15 km s^{-1} (solid line). At short wavelengths, the lines blend into a 'continuum', especially at low resolution.

Table 2. Parameters used for calculations of the hydrogen Pfund lines shown in Fig. 4 (middle panel).

T_e [K]	v_gauss [km s^{-1}]	$A_\mathrm{v}^\mathrm{ISM}$ [mag]	$\int N_\mathrm{e}^2 dV$ [cm^{-3}]
$\leq 10^4$	~ 50	10	$6.35 \cdot 10^{60}$

The interstellar extinction towards MWC 349 is $A_\mathrm{v}^\mathrm{ISM} \simeq 10$ mag. Fitting the observed Pfund lines with the parameters displayed in the left three entries in Table 2 leads to the value of $\int N_\mathrm{e}^2 dV$ in the table, where V is the volume of the emitting region.

The middle panel of Fig. 4 contains the modelled Pfund series added to the continuum emission of MWC 349 (dashed line) taken from Kraus et al. (2000). These two components were subtracted from the observations (upper panel) and the resulting spectrum (lower panel) can be ascribed mainly to CO first overtone band emission. Fitting this CO spectrum is the aim of the following sections.

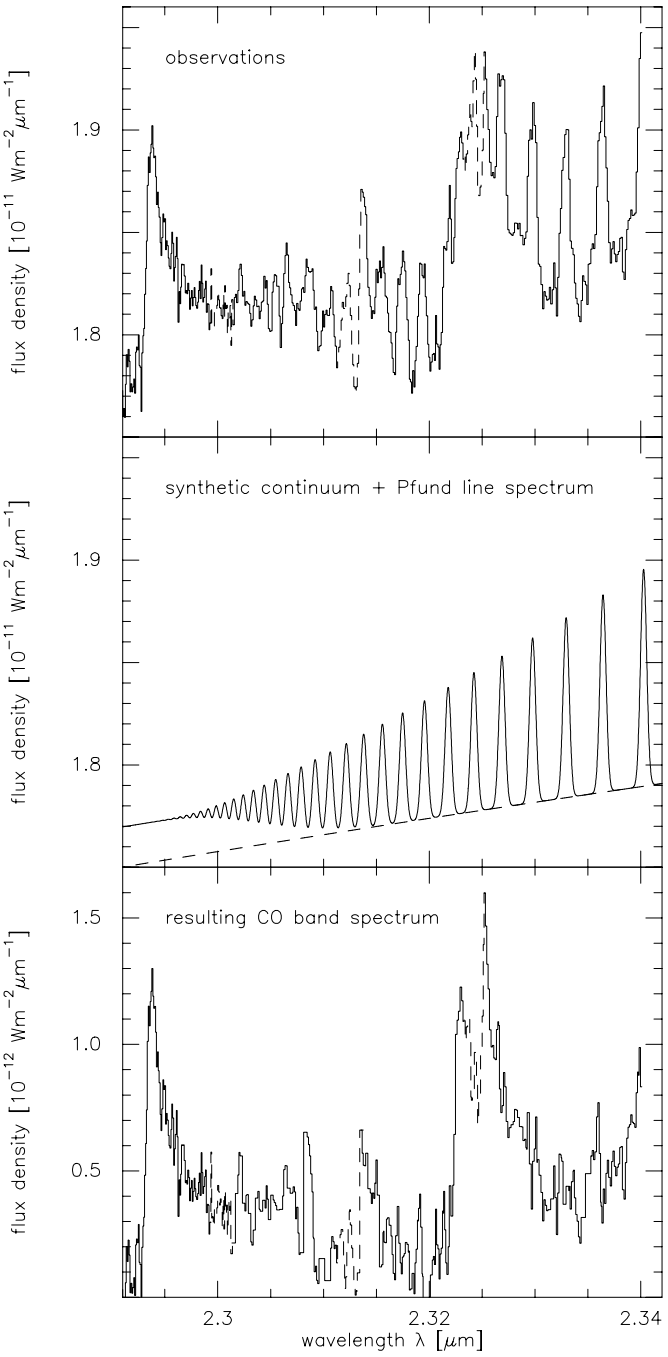

Fig. 4. Subtraction of the synthetic continuum and Pfund line emission (solid line, middle panel, pure continuum is shown by the dashed line) from the observed spectrum (upper panel) leads to the almost pure CO first overtone band emission (lower panel).

4. Modeling the CO band emission

4.1. Theory of the CO bands

The energy of a diatomic molecule in rotational level J and vibrational level v can be expanded in the following way (Dunham 1932a, 1932b)

$$E(v,J) = hc \sum_{k,l} Y_{k,l} \left(v + \frac{1}{2}\right)^k (J^2 + J)^l \,. \qquad (6)$$

For CO the parameters $Y_{k,l}$ are taken from Farrenq et al. (1991). The first overtone bands result from coupled vib-rot transitions in the ground electronic state and obey the selection rules $\Delta v = 2$ and $\Delta J = \pm 1$.

In the following, we assume the CO gas to be in LTE. Then, the levels are populated according to the Boltzmann distribution,

$$N_{vJ} = \frac{N}{Z}(2J+1)\, e^{\frac{-E(v,J)}{kT}} \qquad (7)$$

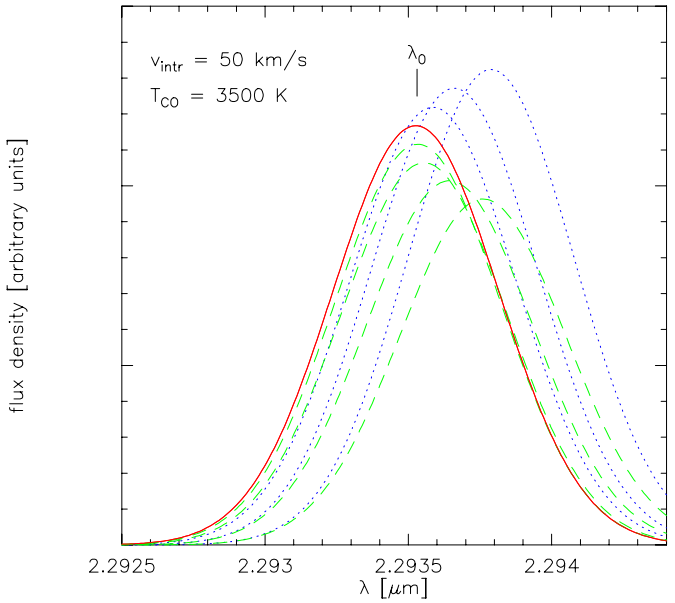

Fig. 5. Individual vib-rot lines that form the $2 \rightarrow 0$ band head. The solid curve is the $(2, 51) \rightarrow (0, 50)$ transition. The dotted curves are the neighbouring transitions with rotational quantum numbers decreasing in steps of one; for the dashed curves, the quantum numbers increase in steps of one.

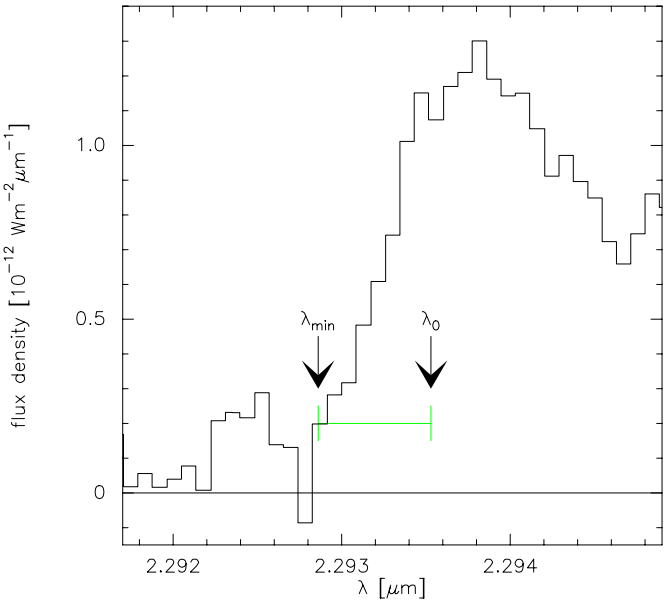

Fig. 6. The onset of the spectrum above noise is choosen as the minimum wavelength $\lambda_{\rm min}$.

where N and T are the total number density and temperature of CO molecules and Z is the total partition function, given as the product of the vibrational and the rotational partition functions

$$Z = Z_v \cdot Z_J = \sum_v e^{\frac{-E_v}{kT}} \cdot \sum_J (2J+1)\, e^{\frac{-E_J}{kT}} \ . \qquad (8)$$

To account for optical depth effects, we calculate the line intensities from the transfer equation

$$I_\nu = B_\nu(T)\,(1 - e^{-\tau_\nu})\,. \qquad (9)$$

The optical depth is $\tau_\nu = \int \kappa_\nu \, ds$ with the absorption coefficient (in cm^{-1}) given by

$$\kappa_\nu = \frac{c^2 N_{vJ} A_{vJ;v'J'}}{8\pi\nu^2} \left(\frac{2j+1}{2j'+1} \cdot \frac{N_{v'J'}}{N_{vJ}} - 1 \right) \Phi_{\rm CO}(\nu) \qquad (10)$$

where $\Phi_{\rm CO}(\nu)$ is the profile function of the CO gas. The Einstein coefficients, $A_{vJ;v'J'}$, are from Chandra et al. (1996).

Let $\lambda_{\rm min}$ denote the onset of the $(2 \rightarrow 0)$ bandhead. We define it to be the wavelength where the intensity of the $(2, 51) \rightarrow (0, 50)$ line (see Fig. 5) has dropped by a factor $x \sim 5$ from its maximum at λ_0; the exact number is not important. We determine $\lambda_{\rm min}$ from Fig. 6 to be $(2.29285 \pm 0.00005)\ \mu$m.

The value of $\lambda_{\rm min}$ depends on the various mechanisms of line broadening. Most processes, such as thermal (turbulent) motion of mean velocity $v_{\rm th}$ ($v_{\rm turb}$), instrumental resolution $v_{\rm res}$, spherical wind $v_{\rm wind}$ (see e.g. Hamann & Simon 1986) lead to gaussian or nearly gaussian line profiles. Their superposition results again in a gaussian line of width $v_{\rm gauss} = \sqrt{v_{\rm th}^2 + v_{\rm turb}^2 + v_{\rm wind}^2 + v_{\rm res}^2}$.

Disk rotation, on the other hand, produces a double-peaked profile. In a gas ring rotating at velocity $v_{\rm rot}$ a line with laboratory frequency ν_0 is shifted up to a maximum frequency $\nu_0 \cdot (1 + v_{\rm rot}/c)$. In a mixture of disk rotation and gaussian broadening one finds the following expression for the minimum wavelength,

$$\frac{1}{\lambda_{\rm min}} = \frac{1}{\lambda_0} \left[1 + \frac{v_{\rm lsr} + v_{\rm rot}}{c} \right] \left[\frac{v_{\rm gauss}}{c} \sqrt{\ln x} + 1 \right] , \qquad (11)$$

where $v_{\rm lsr} = 8\,{\rm km\,s^{-1}}$ is the velocity shift of MWC 349 with respect to the local standard of rest. This relation only holds if the emission contributing to the rise of the spectrum is optically thin. The thermal velocity $v_{\rm th}$ of CO molecules at 3500 K is less than $\sim 1\,{\rm km\,s^{-1}}$ and negligible in comparison with the spectral resolution $v_{\rm res} = 10$–$15\,{\rm km\,s^{-1}}$. The same applies to the turbulent velocity, which is not likely to exceed the speed of sound.

Eq. (11) can be used to relate $v_{\rm wind}$ to the rotational velocity $v_{\rm rot}$. The result is shown in Fig. 7. The dashed lines above and below the solid line are for the lower and upper limit of $\lambda_{\rm min}$. If there is no rotating gas, the inferred wind velocity is about $\sim$50 km s^{-1}, the same velocity as observed for the Pfund lines. If there is no wind the rotation speed of the CO is $\sim 58 \pm 7\,{\rm km\,s^{-1}}$. This value is larger than other rotational velocities around MWC 349 observed up to now, the highest being 42.5 km s^{-1} for He I (Hamann & Simon 1986).

4.2. A gaussian line profile for the CO gas

First, we neglect the effect of rotation and assume a pure gaussian line profile. The velocity of the CO gas, taken from Fig. 7, is $v_{\rm gauss} \approx 50\,{\rm km\,s^{-1}}$.

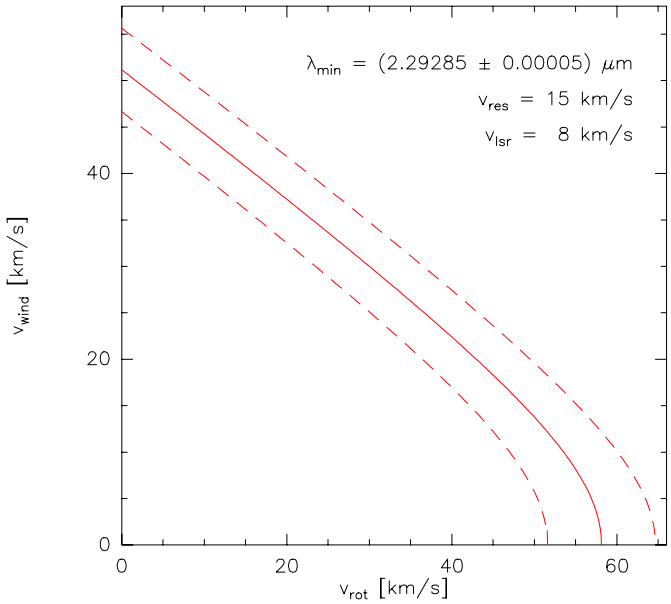

Fig. 7. The dependence of $v_{\rm wind}$ on $v_{\rm rot}$, after Eq. (11), is shown for $x = 10$, and the remaining parameters indicated in the figure. The solid line is for $\lambda_{\rm min} = 2.29285\,\mu$m, the dashed line above (below) is for the lower (upper) limit of $\lambda_{\rm min}$.

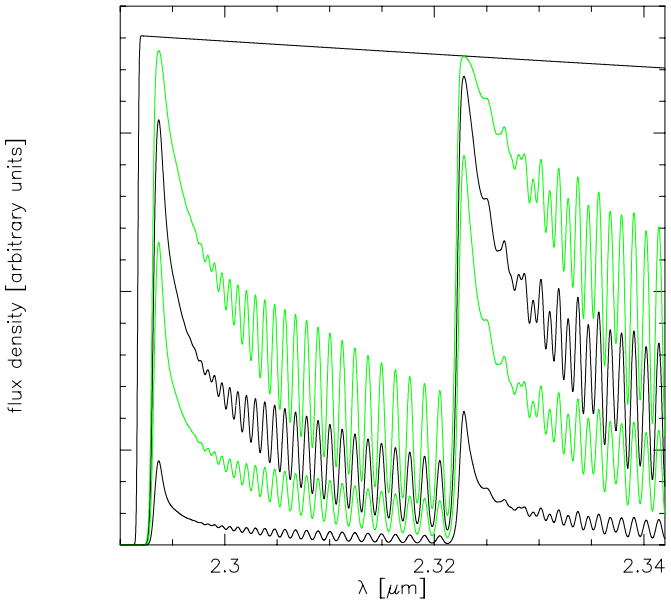

Fig. 9. Calculated CO band emission spectra for $T_{\rm CO} = 4000\,$K, $v_{\rm gauss} \sim 50\,{\rm km\,s^{-1}}$, and $N_{\rm CO}$ increasing from bottom to top: $10^{20}, 5\cdot10^{20}, 10^{21}$, and $2\cdot10^{21}\,{\rm cm^{-2}}$. The upper line represents the case for $\tau \to \infty$.

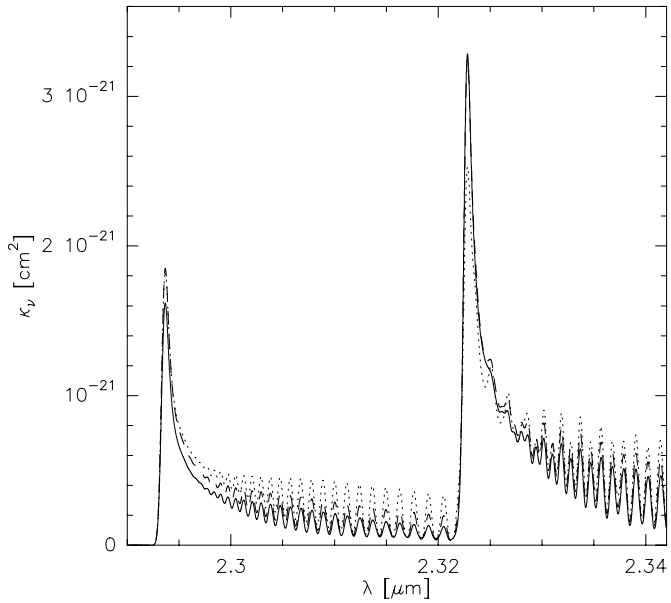

Fig. 8. Absorption coefficient per CO molecule, κ_ν, for temperatures of 3000 K (dotted line), 4000 K (dashed line), and 5000 K (solid line), with $v_{\rm gauss} = 50\,{\rm km\,s^{-1}}$.

For the calculation of the optical depth we assume the absorption coefficient to be constant along the line of sight. Then τ_ν is simply given as the product of the absorption coefficient per CO molecule, κ_ν, times the CO column density, $\tau_\nu = \kappa_\nu \cdot N_{\rm CO}$.

In Fig. 8 we plotted κ_ν for temperatures between 3000 K and 5000 K, and $v_{\rm gauss} = 50\,{\rm km\,s^{-1}}$. In the wavelength range around the $3 \to 1$ band head (2.322–2.325 μm) the absorption coefficient is higher than in the region around the $2 \to 0$ band head (2.293–2.295 μm). This effect becomes stronger with increasing temperature. Thus, the turnover from optically thin to optically thick emission depends not only on the column density but also on the temperature: the $3 \to 1$ band head becomes optically thick at lower temperature and lower column density than the $2 \to 0$ band head.

Next, we vary the CO column density and fix $T_{\rm CO}$ at 4000 K. The synthetic spectra in Fig. 9 are calculated for the case of extreme optical depth (upper line) and for CO column densities (from top to bottom) of $2\cdot10^{21}, 10^{21}, 5\cdot10^{20}$, and $10^{20}\,{\rm cm^{-2}}$. With increasing column density the optical depth increases and the intensity tends towards its limiting blackbody value. In addition, the spectra show two characteristic features: a varying intensity ratio of the two band heads and a broadening of the band head.

The first property can better be seen in Fig. 10 where we plot the flux density ratio of the $3 \to 1$ and $2 \to 0$ band head with temperature for different column densities. This ratio decreases with increasing column density, i.e. increasing τ, and approaches 0.96 for $\tau \to \infty$.

The determination of the column density on the basis of this ratio alone is not unique, because the ratio also depends on temperature, as shown by Fig. 8. Moreover, because the relative strength of the band heads is subject to some uncertainty as discussed in Sect. 2, it does not tightly constrain either parameter.

The second characteristic feature, the broadening of the band head with increasing column density, is largely independent of temperature, as shown in Fig. 8. In Fig. 11 the observed $2 \to 0$ band head region (histogram) is overlaid on model spectra with column densities of $2\cdot10^{21}$ (dashed line), $5\cdot10^{20}$ (solid line), and $10^{20}\,{\rm cm^{-2}}$ (optically thin case, dotted line). The model us-

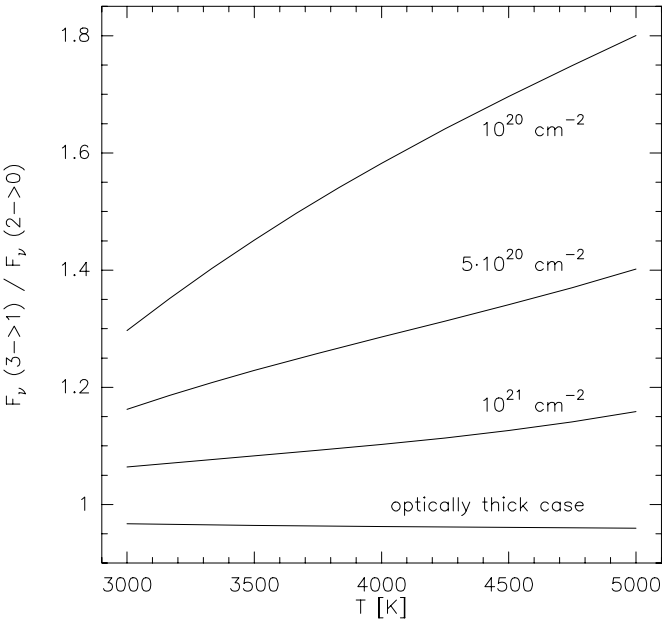

Fig. 10. The flux density ratio of the $3 \rightarrow 1$ and $2 \rightarrow 0$ band heads as a function of temperature and column density. The ratio is highest in the optically thin case ($N_{\rm CO} \leq 10^{20}$ cm^{-2}) and approaches $\simeq 0.96$ for $\tau \rightarrow \infty$.

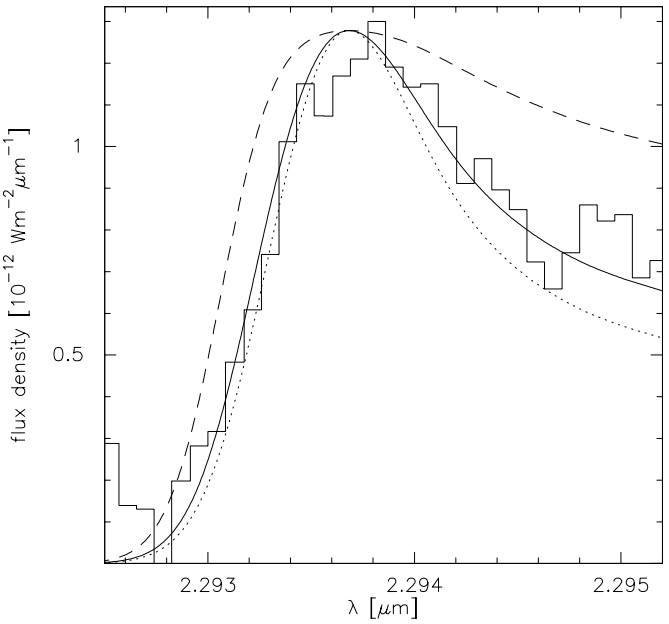

Fig. 11. Theoretical $(2 \rightarrow 0)$ CO band head emission for a gaussian line profile with $v_{\rm gauss} \sim 50\,{\rm km\,s^{-1}}$. The CO column density is $2 \cdot 10^{21}$ cm^{-2} (dashed line), $5 \cdot 10^{20}$ cm^{-2} (solid line) and 10^{20} cm^{-2} (dotted line).

ing the highest column density is clearly unsatisfactory. At first glance, it seems that the observations might also be fitted by optically thin emission, but the upper panel of Fig. 12, which includes a somewhat larger wavelength interval, is clearly inconsistent with the optically thin case whereas the observations can be reconciled with a synthetic spectrum of column density

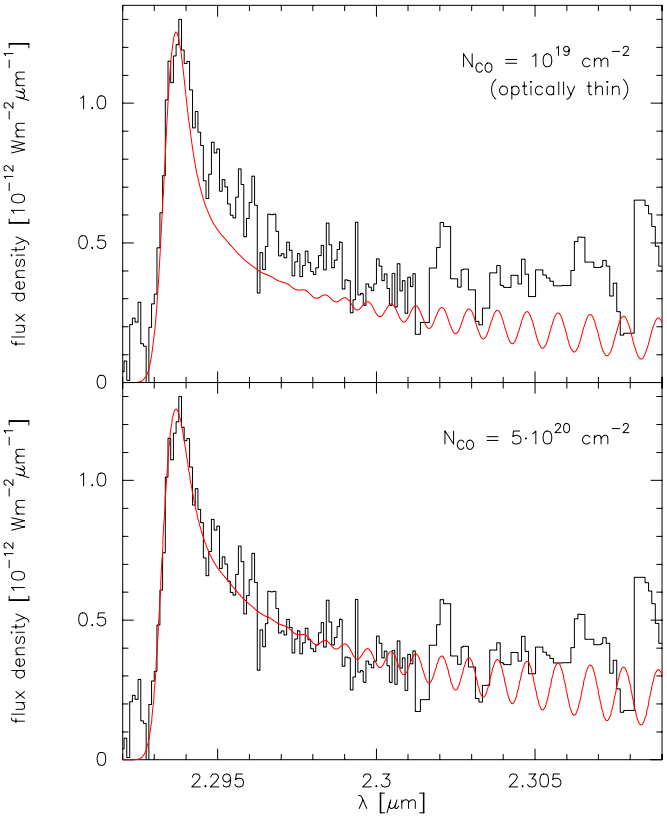

Fig. 12. Comparison between theoretical $(2 \rightarrow 0)$ band head spectra of optically thin (upper panel) and marginally optically thick emission (lower panel). In both cases, the temperature is 3500 K.

$N_{\rm CO} \simeq 5 \cdot 10^{20}$ cm^{-2} (lower panel of Fig. 12). An additional disagreement is that the flux density ratio of the bandheads is highest in the optical thin case and has a value which is inconsistent with the observations.

We conclude that $N_{\rm CO} = 5{\cdot}10^{20}$ cm^{-2} is the best fit CO column density. The synthetic spectra of the $2 \rightarrow 0$ band head look very similar for temperatures in the range of 3000–5000 K. For a more sensitive limitation of the temperature range we examine the $3 \rightarrow 1$ band head. From it we conclude that $T_{\rm CO} = 3500$–4000 K. A more precise determination of the CO temperature requires a high resolution spectrum that covers more than the first two bandheads.

Using the derived values for column density and temperature we model the synthetic CO band spectrum taking into account the foreground extinction, $A_{\rm v}^{\rm ISM}$, and fit it to the observations (Fig. 13; Table 3 summarizes the parameters used). The lower panel of Fig. 13 shows the residue of observed minus calculated spectrum. Some remaining features may result from observational uncertainties (indicated as dashed parts), for example the dip around 2.3225 μm and the region around 2.314 μm, whereas the features at 2.3253 and 2.3084 μm appear to be unidentified emission lines.

For a distance to MWC 349 of 1.2 kpc we find a CO emission area projected on the sky of $A_{\rm CO} \simeq 1.36{\cdot}10^{26}$ cm^2 and $M_{\rm CO} \simeq$

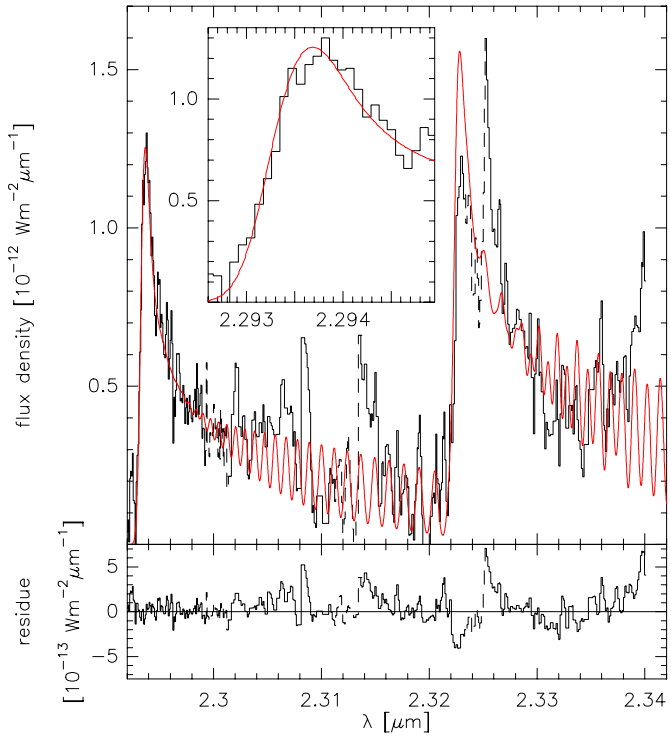

Fig. 13. Modelled CO band emission (solid line) for $T_{\rm CO} = 3500\,{\rm K}$ and $v_{\rm gauss} \sim 50\,{\rm km\,s^{-1}}$ overlaid on the observations (histogram). The model parameters are given in Table 3. The insert shows a blow-up of the $2 \rightarrow 0$ band head. Lower panel: residue of observations minus model. Some yet unidentified emission lines appear to be present.

Table 3. Parameters used for the model spectra shown in Fig. 13. $A_{\rm v}^{\rm ISM}$ denotes the foreground extinction, $A_{\rm CO}$ and $M_{\rm CO}$ are the emitting CO area projected to the sky and the mass of CO derived from the fit, respectively.

$N_{\rm CO}$ [cm^{-2}]	$T_{\rm CO}$ [K]	$v_{\rm gauss}$ [km s^{-1}]	$A_{\rm v}^{\rm ISM}$ [mag]	$A_{\rm CO}$ [cm^2]	$M_{\rm CO}$ [g]
$5 \cdot 10^{20}$	3500	~ 50	10	$1.36 \cdot 10^{26}$	$3.2 \cdot 10^{24}$

$3.2 \cdot 10^{24}$ g. Our value of $A_{\rm CO}$ is about 5 times larger than the lower limit of $2.5 \cdot 10^{25}$ cm^2 found by Geballe & Persson (1987).

4.3. CO bands from a Keplerian disk

We investigate whether the CO bands in MWC 349 also can be successfully modeled as emission from a rotating circumstellar disk. We first calculate the optically thin emission from an infinitesimally narrow ring. For Keplerian rotation, the orbital velocity is

$$v_{\rm rot} = \sqrt{GM_*/r}\,. \tag{12}$$

and the line of sight velocity, $v_{\rm los}$, of a gas element in the ring

$$v_{\rm los} = v_{\rm rot} \cdot \cos\theta \cdot \cos i\,. \tag{13}$$

Here G denotes the gravitational constant, r the ring radius, M_* the stellar mass, i the inclination angle of the ring, and θ the azimuthal angle. The resulting profile of the CO band head smoothed to the instrumantal resolution of $15\,{\rm km\,s^{-1}}$ shows a characteristic shoulder at short wavelengths and a maximum at long wavelengths relative to an unbroadened band head (see Fig. 14). The separation between shoulder and maximum decreases with decreasing orbital velocity. The CO profile of a rotating ring is evidently very different from that observed in MWC 349.

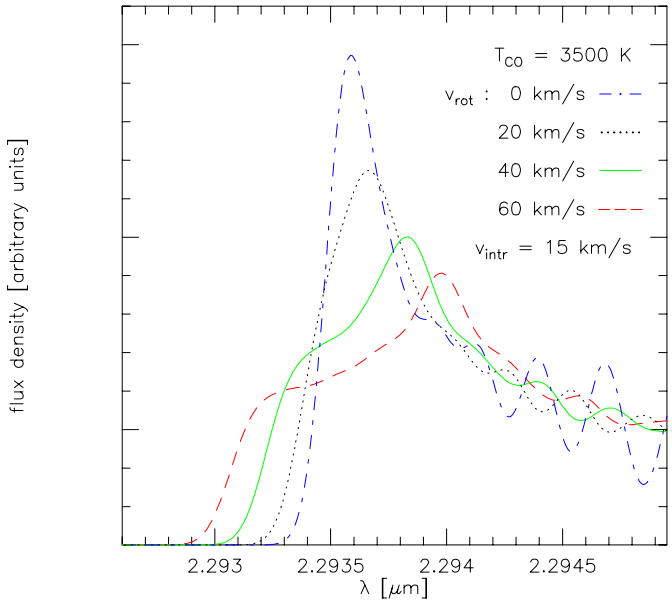

Fig. 14. Optically thin CO band emission from rings of constant rotational velocity ($v_{\rm rot} = 60,\ 40,\ 20$ and $0\,{\rm km\,s^{-1}}$) and for an inclination angle of $i = 0°$. The spectra are smoothed to the instrumental resolution of $15\,{\rm km\,s^{-1}}$.

We next calculate the emission from an entire disk viewed nearly edge-on, using the radiative transfer of Eq. (9). We assume power laws for the temperature and surface density:

$$T(r) \;=\; T_0 \cdot \left(\frac{r}{r_i}\right)^{-p} = T_0 \cdot \left(\frac{v}{v_i}\right)^{2p} \tag{14}$$

$$\Sigma(r) \;=\; \Sigma_0 \cdot \left(\frac{r}{r_i}\right)^{-q} = \Sigma_0 \cdot \left(\frac{v}{v_i}\right)^{2q} \tag{15}$$

Here r_i is the inner radius of the Keplerian disk where the rotational velocity has its maximum value v_i. We fix the inner radius by putting $v_i = 60\,{\rm km\,s^{-1}}$ (see Fig. 7). Further, we assume $T_0 = 5000\,{\rm K}$, which is the dissociation limit of CO molecules, and an inclination angle of $10°$. The radius $r_{\rm out}$, out to which the CO (2→1) band is thermally excited, is a free parameter; the velocity there we denote as $v_{\rm out}$. For these disk calculations we surmise that the first overtone bands are subthermally excited for radii greater than $r_{\rm out}$, due to lower densities. Therefore the contribution of CO beyond $r_{\rm out}$ to the overall spectrum is small. The CO disk is geometrically flat so that along each line of sight through the inclined disk the density and temperature are constant. The total flux from the disk is obtained by straightforward numerical integration.

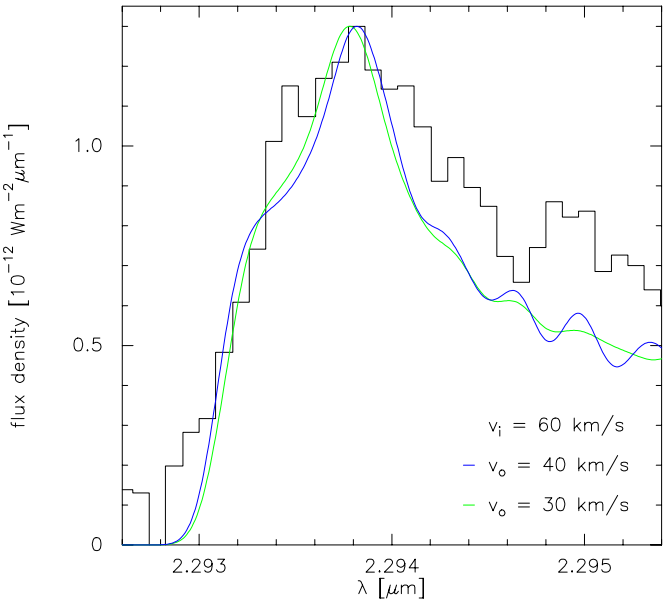

Fig. 15. Best fit model spectrum (histogram) for a Keplerian disk. Model parameters from Table 4.

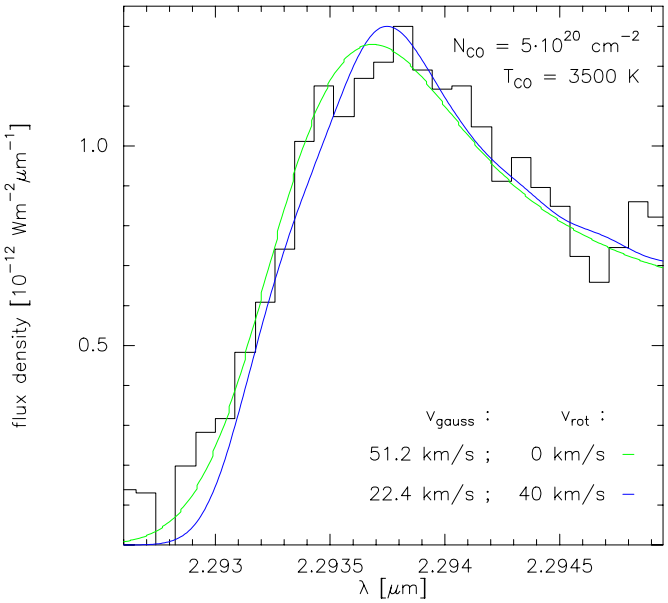

Fig. 16. Best fits to the observed $2 \rightarrow 0$ band head. The light line represents the pure gaussian fit of Fig. 13 and the dark line shows the combination of a rotational component and a gaussian velocity component whose velocities are determined according to Eq. 11.

Table 4. Parameters of the best fit model spectrum for a CO disk, shown in Fig. 15. Fixed parameters are $M_* = 26\,M_\odot$, $T_0 = 5000$ K, $p = 0.5$, $q = 1.5$, and $v_i = 60\,\mathrm{km\,s^{-1}}$ which leads to $r_i \simeq 6.4$ AU.

$v_{\rm out}$ [km s^{-1}]	$r_{\rm out}$ [AU]	$T(r_{\rm out})$ [K]	N_0 [cm^{-2}]	$N(r_{\rm out})$ [cm^{-2}]
40	14.4	3333	$8.5 \cdot 10^{16}$	$2.5 \cdot 10^{16}$
30	25.6	2500	$5.8 \cdot 10^{16}$	$7.3 \cdot 10^{15}$

By a systematic variation of the free parameters ($\Sigma_0, v_{\rm out}, p, q$), we find that the shape of the spectrum is strongly influenced by the column density at the inner edge and by the size of the disk, whereas the exponents p and q play a minor role; we therefore fix them following Hayashi (1981) to $p = 0.5$ and $q = 1.5$. Similar numbers are derived for the dust disk (Kraus et al. 2000).

The disk models then contain only two free parameters: the outer radius, $r_{\rm out}$, and the column density at the inner edge, N_0. To explain the observed band head profile with a rotating disk, a large spread in the rotational velocity is required; the shoulders seen in Fig. 14 are not sufficiently suppressed. The large velocity spread implies a large emitting area, and therefore a low column density, so that the emission becomes very optically thin ($\tau \simeq 10^{-4}$), even at the inner edge of the CO disk. The outer velocity $v_{\rm out}$ must lie in the range between 30 and 40 km s^{-1}. If $v_{\rm out}$ were greater, the shoulder of the band head would become too broad; if it were less, the profile would be too narrow. Our best models of a rotating disk are presented in Fig. 15. Considering the quality of the data, they are only marginally acceptable.

We add that if one assumes the dust and gas to be thermally decoupled, it still is possible in the models for the strength of the CO band head to be $f \sim 5\,\%$ of the continuum, as observed, although the CO emission is very optically thin. As the dust emits like a blackbody, the equation $f\,B_\nu(T_d) = \tau_\nu\,B_\nu(T_{\rm CO})$ is approximately fulfilled for $T_d \sim 1000$ K, $T_{\rm CO} \sim 4000$ K and $\tau \sim 10^{-4}$.

5. Discussion

Mathematically, there is also the possibility of combining the wind model of Fig. 11 (solid line), which is based on a gaussian profile of ~ 50 km s^{-1} half width, with Keplerian rotation, as long as $v_{\rm rot} \leq 40$ km s^{-1}. This is shown in Fig. 16 (black curve), where a rotational component with $v_{\rm rot} = 40$ km s^{-1} is added to the gaussian velocity profile. Otherwise the basic parameters are the same as for the wind (LTE; CO column density $\sim 5 \cdot 10^{20}$ cm^{-2}; $T_{\rm CO} = 3500$–4000 K).

Although the fit is again very good, this scenario has the following difficulties: If $v_{\rm rot} \leq 40$ km s^{-1}, the stellar mass of 26 M$_\odot$ implies a distance greater than 14 AU. If the CO gas is coupled to the dust, it should have the same temperature of ~ 950 K as the dust grains at that distance (Kraus et al. 2000), which is much too low. If CO is located above the disk and thermally decoupled from the dust, it might achieve the required temperature of ~ 3500 K by radiative heating. But the CO column density of $5 \cdot 10^{20}$ cm^{-2} then implies a gas surface density which is at least an order of magnitude greater than that implied by the dust disk (adopting standard conversion factors $\Sigma_{\rm dust} : \Sigma_{\rm H} \simeq 10^{-2}$, $N_{\rm CO} : N_{\rm H} \simeq 10^{-4}$).

The scenario of a pure wind is very vague in its details, but gives a remarkably good fit. We might think of dense molecular blobs emanating from the disk. The total emission area of the blobs is ~ 0.6 AU^2.

There is yet another alternative with $N_{\rm CO} \sim 5 \cdot 10^{20}$ cm^{-2}, which we discuss now. If the CO band emission arises in the

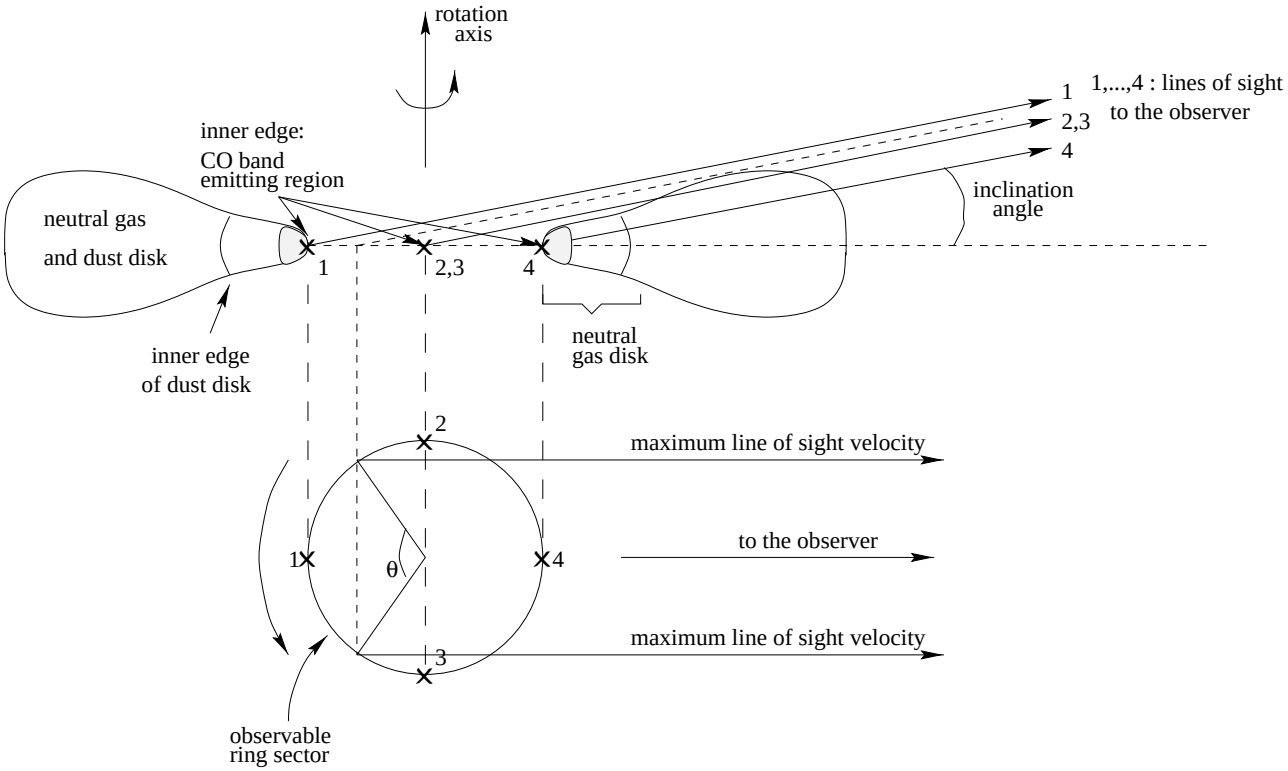

Fig. 17. Sketch of the disk around MWC 349 seen edge on, which includes a bulging neutral outer region where dust has condensed. Because of the small inclination angle, only emission from sector 1 where the radial velocity is small will reach the observer. Radiation from other locations, for example, from the points marked 2, 3, and 4, is absorbed by the bulge.

disk, it must come from inside the evaporation radius of the dust because of its high temperature ($\sim$ 3500 K). According to the Kraus et al. model of the dust disk, the distance is then smaller than 2.88 AU implying a rotational velocity greater than 90 km s^{-1}. We assume $v_{\rm rot} \simeq 100$ km s^{-1}. To avoid the problems with the line profile in case of such a high $v_{\rm rot}$, as discussed in Sect. 4.3 and demonstrated in Fig. 14, we propose a configuration as depicted in Fig. 17. The outer dusty part of the disk has a bulge and, because of its small inclination angle $i \sim 10°$, this bulge blocks the light from the inner edge of the disk on the near side to the observer. We therefore receive emission only from sector 1 in Fig. 17 where the *radial* velocity is low. In Fig. 18 we show computations of the flux received from sector 1 for different opening angles θ. The ranges of radial velocities in the sectors are summarized in Table 5.

Table 5. Angles θ and velocity ranges $v_{\rm rot,los}$ for the calculated sectors shown in Fig. 18. The inclination angle is taken as 10° and the rotational velocity is 98 km s^{-1}.

	θ[°]	$v_{\rm rot,los}$[km s^{-1}]
dashed line	180	$-96.5 \ldots 96.5$
solid line	75	$-59.0 \ldots 59.0$
dotted line	33	$-27.6 \ldots 27.6$

6. Conclusions

We have presented low and high resolution spectra in the near infrared of the B[e]-star MWC 349. The wavelength interval 2.285–2.342 μm, observed at high spectral resolution, contains mainly emission by the first overtone bands of the CO molecule as well as the Pfund series of atomic hydrogen. From modeling the Pfund lines under the assumption that they are optically thin, we find that they come from the inner part of the H II region around MWC 349 and are in LTE. The hydrogen line profiles are approximately gaussian and their widths indicates a wind speed of ~ 50 km s^{-1}.

The observed CO is at a temperature of 3500–4000 K, and the population of the vibrational levels is close to LTE. The width of the $2 \rightarrow 0$ band head indicates a velocity broadening of the order of 50–60 km s^{-1}, depending on the broadening mechanism, wind or rotation. The location of the hot CO gas producing the band emission could not be conclusively identified, but several scenarios are possible while others can be nearly ruled out.

Because the CO as well as the Pfund lines can be fitted with a gaussian velocity component of ~ 50 km s^{-1}, the one possibility is that the CO bands arise in the windy transition layer between the disk and the H II region, presumably in dense clumps. In this case the band head has an optical depth of order unity ($N_{\rm CO} \simeq 5 \cdot 10^{20}$ cm^{-2}).

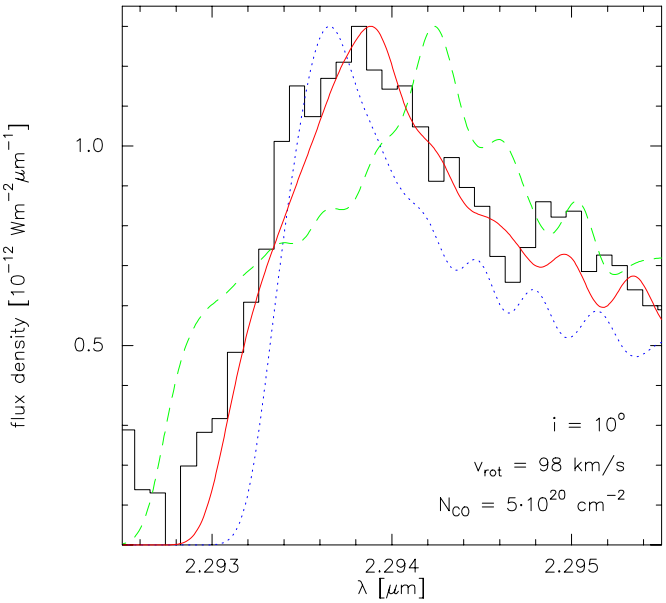

Fig. 18. Fit to the observed $2 \rightarrow 0$ band head for ring segments with a Keplerian velocity of $v_{\rm rot} \simeq 100\,{\rm km\,s^{-1}}$. The geometry is depicted in Fig. 17. The angles and the corresponding velocity ranges are given in Table 5. The best fit is shown by the solid line.

Alternatively, the CO emits in a thin layer above the dust disk at radii between 6.5 and 15 AU. In this scenario, the CO emission is optically very thin ($N_{\rm CO} \simeq 6 \cdot 10^{16}\,{\rm cm^{-2}}$; $\tau \simeq 10^{-4}$), and the gas is thermally decoupled from the dust. As we could only produce spectral fits of mediocre quality (see Fig. 15), due to the characteristic line profiles under Keplerian rotation (see Fig. 14), this does not appear to be a likely configuration.

Finally, we suggest that the CO bands come from the inner edge of the circumstellar disk. Because of the required high temperature and column density, the CO gas must be located inside the evaporation radius of the dust, i.e. at distances less than ~ 3 AU from the star. This implies a high rotational speed and a characteristic shoulder in the profile of the band head, which is not observed. To suppress the shoulder the disk must have an outer bulge, as depicted in Fig. 17, where dust can absorb the CO line emission from the near inner edge of the disk. In this case the observer sees CO only in a sector on the far side of the disk where radial velocities are smaller than $\sim 60\,{\rm km\,s^{-1}}$. With such a geometrical configuration, a satisfactory fit is also possible (see Fig. 18).

Acknowledgements. The United Kingdom Infrared Telescope is operated by the Joint Astronomy Centre on behalf of the U. K. Particle Physics and research Council. We would like to thank Frank Shu, the referee, for his helpful comments.

References

Calvet, N., Patiño, A., Magris, C.G., D'Alessio, P., 1991, ApJ 380, 617
Carr, J.S., 1989, ApJ 345, 522
Carr, J.S., 1995, Ap & SS 224, 25
Carr, J.S., Tokunaga, A.T., Najita, J., Shu, F.H., Glassgold, A.E., 1993, ApJ 411, L 37
Chandler, C.J., Carlstrom, J.E., Scoville, N.Z., Dent, W.R., Geballe, T.R., 1993, ApJ 412, L 71
Chandler, C.J., Carlstrom, J.E., Scoville, N.Z., 1995, ApJ 446, 793
Chandra, S., Maheshwari, V.U., Sharma, A.K., 1996, A&AS 117, 557
Cohen, M., Bieging, J.H., Dreher, J.W., Welch, W.J., 1985, ApJ 292, 249
Dunham, J. L., 1932a, Phys.Rev. 41, 713
Dunham, J. L., 1932b, Phys.Rev. 41, 721
Farrenq, R., Guelachvili, G., Sauval, A. J., Grevesse, N., Farmer, C. B., 1991, J.Mol.Spectrosc. 149, 375
Geballe, T.R., Persson, S.E., 1987, ApJ 312, 29
Geisel, S.L., 1970, ApJ 161, L 105
Green, T.P., Lada, C.J., 1996, ApJ 461, 345
Hamann, F., Simon, M., 1986, ApJ 311, 909
Hamann, F., Simon, M., 1988, ApJ 327, 876
Hayashi, C., 1981, Suppl.Prog.Theor.Phys. 70, 35
Kraus, M., 2000, PhD-Thesis, University of Bonn
Kraus, M., Krügel, E., Hengel, C., Thum, C., 2000 *in preparation*
Lamers, H.J.G.L.M., Zickgraf, F.-J., de Winter, D., Houziaux, L., Zorec, J., 1998, A&A 340, 117
Leinert, C., 1986, A&A 155, L 6
Mariotti, J.M., Chelli, A., Foy, R., Léna, P., Sibille, F., Tchountonov, G., 1983, A&A 120, 237
Martin, S.C., 1997, ApJ 478, L 33
Martín-Pintado, J., Bachiller, R., Thum, C., Walmsley, M., 1989, A&A 215, L 13
Menzel, D.H., Pekeris, C.L., 1935, MNRAS 96, 77
Najita, J., Carr, J.S., Glassgold, A.E., Shu, F.H., Tokunaga, A.T., 1996, ApJ, 462, 919
Rodríguez, L.F., Bastian, T.S., 1994, ApJ 428, 324
Scoville, N., Hall, D.N.B., Kleinmann, S.G., Ridgeway, S.T., 1979, ApJ 232, L 121
Smith, H.A., Strelnitski, V., Miles, J.W., Kelly, D.M., Lacy, J.H., 1997, AJ 114, 2658
Storey, P.J., Hummer, D.G., 1995, MNRAS 272, 41
Strelnitski, V.S., Haas, M.R., Smith, H.A., Erickson, E.F., Colgan, S.W.J., Hollenbach, D.J., 1996, Sci 272, 1459
Thum, C., Martín-Pintado, J., Bachiller, R., 1992, A&A 256, 507
Thum, C., Martín-Pintado, J., Quirrenbach, A., Matthews, H.E., 1998, A&A 333, L 63
Thum, C., Matthews, H.E., Martín-Pintado, J., Serabyn, E., Planesas, P., Bachiller, R., 1994, A&A 283, 582
Thum, C., Strelnitski, V.S., Martín-Pintado, J., Matthews, H.E., Smith, H.A., 1995, A&A 300, 843
White, R.L., Becker, R.H., 1985, ApJ 297, 677